ACS MATERIALS LETTERS

www.acsmaterialsletters.org

Perovskite Quantum Dot Solar Cells Fabricated from Recycled Lead-Acid Battery Waste

Long Hu, Qingya Li, Yuchen Yao, Qiang Zeng, Zizhen Zhou, Claudio Cazorla, Tao Wan, Xinwei Guan, Jing-Kai Huang, Chun-Ho Lin, Mengyao Li, Soshan Cheong, Richard D. Tilley, Dewei Chu, Jianyu Yuan,* Shujuan Huang, Tom Wu,* and Fangyang Liu*

Cite This: *ACS Materials Lett.* 2022, 4, 120−127

Read Online

ABSTRACT: A cost-effective and environmentally friendly Pb source is a prerequisite for achieving large-scale, low-cost perovskite photovoltaic devices. Currently, the commonly used method to prepare the lead source is based on a fire smelting process, requiring a high temperature of more than 1000 °C, which results in environmental pollution. Spent car lead acid batteries are an environmentally hazardous waste; however, they can alternatively serve as an abundant and inexpensive Pb source. Due to "self-purification", quantum dots feature a high tolerance of impurities in the precursor since the impurities tend to be expelled from the small crystalline cores during colloidal nucleation. Herein, PbI_2 recycled from spent lead acid batteries via a facile low-temperature solution process is used to synthesize $CsPbI_3$ quantum dots, which simultaneously brings multiple benefits including (1) avoiding pollution originating from the fire smelting process; (2) recycling the Pb waste from batteries; and (3) synthesizing high-quality quantum dots. The resulting $CsPbI_3$ quantum dots have photophysical properties such as PLQY and carrier lifetimes on par with those synthesized from the commercial PbI_2 due to expelling of the impurity Na atoms. The resulting solar cells deliver comparable power conversion efficiencies: 14.0% for the cells fabricated using recycled PbI_2 and 14.7% for the cells constructed using commercial PbI_2. This work paves a new and feasible path to applying recycled Pb sources in perovskite photovoltaics.

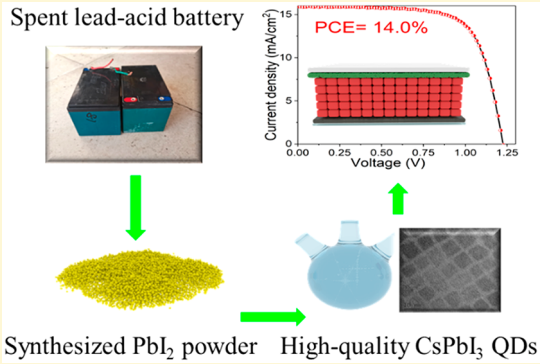

Colloidal quantum dots (QDs) have demonstrated unique photophysical features such as size-dependent tunable absorption and efficient multiple exciton, which make them promising candidates for a wide range of applications in photovoltaics, light emitting diodes and photodetectors.[1−9] In the past decade, the device performance and stability of Pb chalcogenide QD solar cells have been significantly improved through optimizing synthesis methods, designing device architectures, and engineering defect passivation.[10−16] To date, the champion PbS and PbSe QD solar cells have enabled power conversion efficiencies (PCEs) of 13.8%[17] and over 10%,[4,18,19] respectively. Recently, inorganic lead halide perovskite $CsPbI_3$ QDs have risen as a superstar for optoelectronic applications because they exhibited near-unity photoluminescence quantum yield (PLQY) and high defect-tolerance, which provide an attractive platform to further boost the efficiency of QD solar cells.[20−27] Additionally, $CsPbI_3$ QDs demonstrate robust mechanical properties under bending due to their nanoscale crystalline grains.[28] More importantly, $CsPbI_3$ QDs exhibit significantly enhanced phase stability at room temperature in comparison with their bulk counterparts, which offers a significant opportunity for improving the lifetime of perovskite QD solar cells.[29−32] To date, $CsPbI_3$ QD solar cells have shown a great potential for high-performance and low-cost photovoltaics.[30,33−36]

Pb element is indispensable for achieving highly efficient and stable QD solar cells since Pb-related orbitals dominate the conduction band (CB) edges and play an important role in the charge transport of QDs.[8] However, the toxicity of Pb has

Received: September 24, 2021
Accepted: December 2, 2021

https://doi.org/10.1021/acsmaterialslett.1c00592
ACS Materials Lett. 2022, 4, 120−127

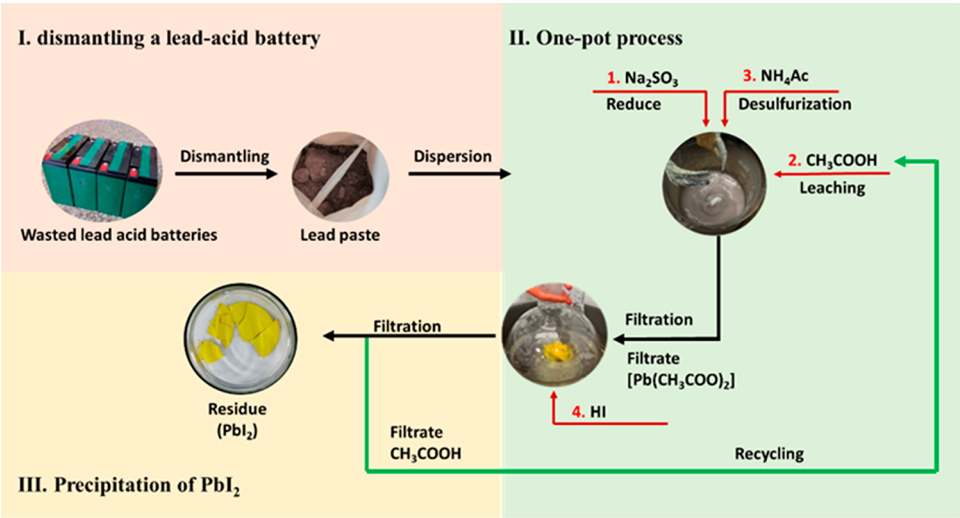

Figure 1. Process flow of recycling the Pb source from spent lead-acid batteries.

always been a cause of concern for the perovskite commercial applications. Reducing leakage and improving recycle efficiency of Pb are the two main solutions for addressing the lead toxicity concern and the environmental pollution.[37] Currently, it is a common process to prepare lead ingots in lead regeneration through the fire smelting process.[38] However, lead composites such as lead sulfate require a high temperature of more than 1000 °C to be decomposed, which results in environmental pollution due to the emission of lead particles and sulfur dioxide into the atmosphere. Another effective and straightforward strategy for reducing environmental pollution is to find alternative lead sources that are abundant, inexpensive, and allow safe extraction and processing procedures.[39] Lead-acid batteries are widely used in automotive vehicles, which produce massive environmentally hazardous wastes including Pb anodes and cathodes after retirement. These hazardous Pb electrodes are required to be disposed or reprocessed appropriately.[37] Therefore, the recovery of lead-acid batteries provides an alternative and readily available lead source for fabricating Pb-based solar cells.

In a pioneering work, Chen et al. utilized PbI_2 extracted from lead-acid batteries to fabricate $MAPbI_3$ halide perovskite solar cells and achieved a PCE of 9.37%.[38] Very recently, Li et al. further improved the efficiency of $MAPbI_3$ halide perovskite solar cells to over 17% using recycled $Pb(Ac)_2$ from lead-acid batteries. These achievements prove that the lead source from lead-acid batteries could be used in halide perovskite thin-film photovoltaics.[40] However, the device performance in these works is far inferior to those fabricated from commercial PbI_2 due to the presence of impurity elements in the recycled lead source. In addition, the above-reported methods still require high-temperature sintering processes (>500 °C) to extract Pb from the spent lead acid batteries. Therefore, there is an urgent need to develop a safe approach of low-temperature recycling of Pb and to fill the efficiency gap between conventional and recycled perovskite photovoltaics.

In contrast to the bulk film counterpart, perovskite QDs in principle feature a high tolerance of impurities in the precursor since the impurities tend to be expelled from the small crystalline cores during colloidal nucleation, thus reducing the possibility of defect formation.[41] Therefore, the recycled Pb source with low purity and cost is more favorable to synthesize perovskite QDs for optoelectronic device fabrication. In this work, we conceived a facile low-temperature solution process and successfully extracted Pb source from spent car lead-acid batteries to synthesize PbI_2 powders. The obtained PbI_2 was further utilized to synthesize $CsPbI_3$ QDs, which demonstrated similar photophysical performance including PLQY and carrier lifetime compared to those synthesized from commercial PbI_2. The champion solar cell fabricated from the recycled PbI_2 achieved a high PCE of 14.0%, which is comparable to the 14.7% efficiency of the solar cell made from the commercial PbI_2. These results endorse the effectiveness of the proposed low-temperature solution process for reusing waste Pb and validates the compatibility of recycled Pb source to synthesize high-quality perovskite QDs for efficient optoelectronics, which not only reduces the lead waste issue but also promotes the added value of spent batteries.

Figure 1 illustrates the low-temperature recycling process using waste anodes and cathodes collected from spent car batteries to produce PbI_2 end-product. First, a spent lead acid battery was dismantled, and then the acid electrolyte that contains concentrated sulfuric acid was diluted with water and poured out. The electrodes were further rinsed with water several times and air-dried. The anode and cathode materials were mixed for preparing lead paste, which contains $PbSO_4$, PbO_2, and PbO components. To understand the composition of lead paste, ethylenediaminetetraacetic acid (EDTA) complexometric titration was employed for analyzing the content of chemical components.[42] The weight content of lead paste is 16.6% for PbO, 32.03% for PbO_2, and 17.71% for $PbSO_4$. Afterward, we introduced a facile one-pot solution process to extract the Pb source by mixing lead paste (5 g) with excess Na_2SO_3 (1 g), dilute acetic acid (Ac, 80 mL, 0.4 mmol/mL), and ammonium acetate (NH_4Ac, 0.5 g). Subsequently, the mixture was stirred at 35 °C for 24 h to form lead acetate. After sufficient reaction, the mixture was filtered to obtain a clear lead acetate solution. Then excess hydroiodic acid (HI) was added slowly to the lead acetate solution under stirring, and the formation of yellow PbI_2 precipitate was observed. The yellow solid was collected and dried in vacuum at 60 °C overnight. The detailed reactions of proposed low-temperature recycling are as follows (eqs 1−4):

$$PbO_2 + Na_2SO_3 — PbO + Na_2SO_4 \quad (1)$$

https://doi.org/10.1021/acsmaterialslett.1c00592
ACS Materials Lett. 2022, 4, 120−127

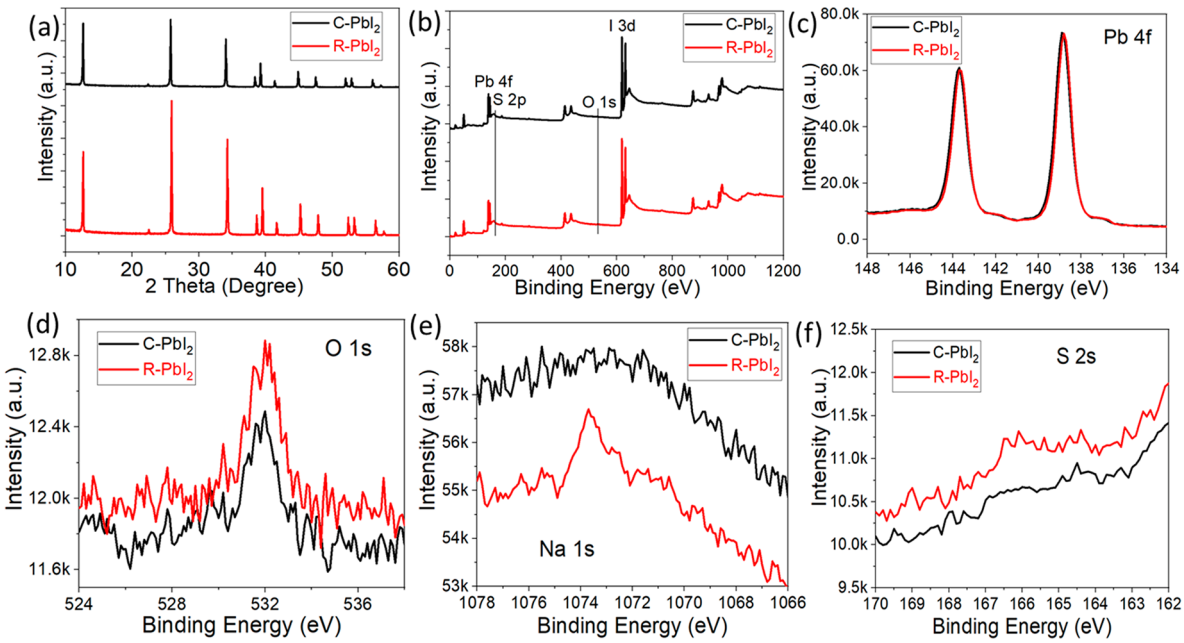

Figure 2. Crystallinity and composition characterizations of C−PbI_2 and R−PbI_2. (a) XRD patterns of C−PbI_2 and R−PbI_2. (b) Full XPS spectra of C−PbI_2 and R−PbI_2. Core XPS spectra of C−PbI_2 and R−PbI_2 in (c) Pb 4f, (d) O 1s, (e) Na 1s, and (f) S 2s binding energy ranges.

$$PbO + 2HAc — PbAc_2 + H_2O \quad (2)$$

$$PbSO_4 + 2NH_4Ac — PbAc_2 + (NH_4)_2SO_4 \quad (3)$$

$$PbAc_2 + 2HI — PbI_2 + 2HAc \quad (4)$$

The as-obtained PbI_2 powder was characterized to confirm its crystal structure and purity, which is a prerequisite for synthesizing high-quality $CsPbI_3$ QDs. As a comparison, commercial PbI_2 (Sigma) was also used to fabricate perovskite QD solar cells, and the recycled and commercial PbI_2 were denominated as R−PbI_2 and C−PbI_2, respectively. Figure 2a shows the X-ray powder diffraction (XRD) patterns of both R−PbI_2 and C−PbI_2. Both PbI_2 present identical XRD patterns and no impurity phase is observed, indicating successful synthesis of fine crystalline PbI_2 from the waste lead acid battery.[43,44] To further verify the purity of PbI_2, X-ray photoelectron spectrum (XPS) measurement was conducted to investigate the elemental composition, valence states, and atomic ratio.[45] Figure 2b illustrates the full XPS spectra of both kinds of PbI_2, while Figure 2c−f give the core XPS spectra of Pb 4f, O 1s, Na 1s, and S 2s, respectively. For the core XPS spectra of Pb 4f (Figure 2c), two main peaks are observed at 144.2 and 138.9 eV, which are assigned to the Pb 4f 5/2 and Pb 4f 7/2, respectively.[46] Notably, no peaks were observed at any lower binding energy near the main signals, which suggests the absence of metallic Pb atoms and confirms the purity of PbI_2.[47] Figure 2d shows that the O 1s peak in the R−PbI_2 is higher than that in the C−PbI_2. Furthermore, Figure 2e,f points out the existence of Na and S elements in the R−PbI_2. Combining the XPS results of O, Na, and S elements, we can conclude that the Na_2SO_3 component was not completely removed from the end-product R−PbI_2. The atomic ratios in both kinds of PbI_2 are summarized in Table 1, in which the high similarity in the elemental composition endorses the application of R−PbI_2 in widespread usages.

Undesirable impurity elements in bulk perovskite thin film usually create defect states and retard their optoelectronic performance severely due to nonradiative recombination.[48,49] On the other hand, colloidal perovskite QDs own a different nucleation mechanism and the famous self-purification effect is regarded as a significant advantage of colloidal synthesis, in which the impurities are easier to be expelled from the nanoscale nucleation cores.[41,50] Therefore, colloidal perovskite QDs should possess better compatibility with a recycled lead source for high-performance and less polluted optoelectronic applications. As comparison, both C−PbI_2 and R−PbI_2 were employed to synthesize $CsPbI_3$ QDs using a hot-injection method. Briefly, 0.5 g of PbI_2, 2.5 mL of oleic acid (OA), and 25 mL of octadecene (ODE) were loaded in 100 mL three-neck flask and vacuum pumped under continuous stirring at 100 °C for 1 h. Then, 2.5 mL of oleylamine (OLA) was injected into the flask. After PbI_2 completely dissolved, the temperature was increased to 160 °C under a N_2 flow protection. A volume of 4 mL of Cs-OA precursor solution was injected swiftly into the flask and reacted for 5 s, and the solution was quenched by an ice bath. All synthesis conditions were identical except the PbI_2 source for both batches of $CsPbI_3$ QDs. The crude $CsPbI_3$ QDs solution was evenly divided into three centrifugation tubes, and then methyl acetate was added into tubes with a volume ratio of 1:3 (QD solution−methyl acetate). Subsequently, QD precipitate was extracted by centrifugation at the speed of 8000 rpm for 3 min. All of the QD precipitate in three tubes was dispersed with 3 mL of hexane and then precipitated by adding 4.5 mL of methyl acetate and centrifuged again at 8000 rpm for 3 min. Finally, the extracted QDs were dissolved in hexane for characterizations and device fabrication.

Table 1. Atomic Ratios of C−PbI_2 and R−PbI_2 Obtained from XPS Results

PbI_2 type	Pb	S	O	Na	I	C
C−PbI_2	20.24	2.08	2.69	0.00	58.79	16.20
R−PbI_2	20.01	2.47	3.01	0.50	57.98	15.96

https://doi.org/10.1021/acsmaterialslett.1c00592
ACS Materials Lett. 2022, 4, 120−127

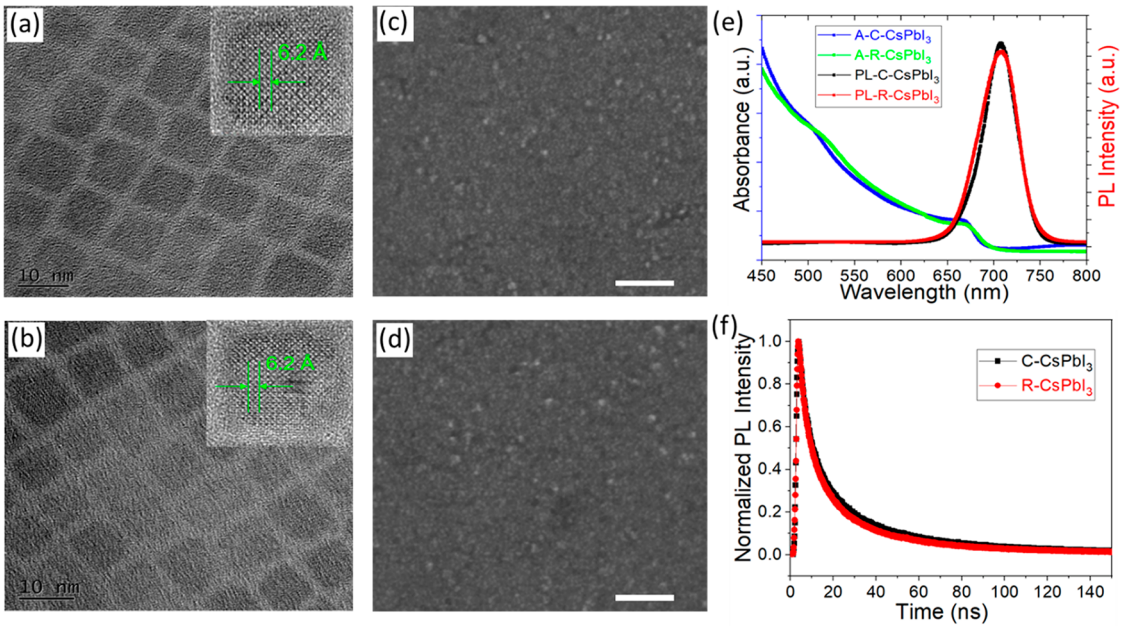

Figure 3. TEM images of (a) C−$CsPbI_3$ and (b) R−$CsPbI_3$ QDs. SEM images of (c) C−$CsPbI_3$ and (d) R−$CsPbI_3$ QD films; scale bar, 300 nm. (e) Steady-state PL and absorbance spectra of C−$CsPbI_3$ and R−$CsPbI_3$ QD films. (f) Time-resolved PL spectra of both QD films.

Both kinds of $CsPbI_3$ QDs were thoroughly characterized. Transmission electron microscopy (TEM) images of C−$CsPbI_3$ (synthesized from C−PbI_2) and R−$CsPbI_3$ QDs (synthesized from the R−PbI_2) in Figure 3a,b, respectively, show that both batches of QDs formed in cubic shape with an average size of 9 nm. High-resolution TEM images of both QDs (see the insets in Figure 3a,b) confirm the formation of the cubic phase of $CsPbI_3$ with the measured lattice spacings of 6.2 Å corresponding to the ⟨100⟩ planes. The PLQY measurement provides valuable insight on the defect density, and a higher PLQY often indicates a lower defect density due to suppressed nonradiative recombination. Both batches of $CsPbI_3$ QDs feature quite comparable PLQY, i.e., 92% for the C−$CsPbI_3$ and 90% for the R−$CsPbI_3$ QDs, which are on par with the reported values.[51−53] Therefore, it can be concluded that both kinds of $CsPbI_3$ QDs share similar characteristics including size distribution and defect density. In addition, the Na element in R−$CsPbI_3$ QDs was not detected in XPS results, as shown in Figure S1, implying that Na atoms were expelled out from $CsPbI_3$ QDs due to the self-purification effect.

Both types of $CsPbI_3$ QD solution were spin-coated on the SnO_2 nanoparticle (NPs)/ITO substrates and treated with methyl acetate to form dense semiconducting QD films. The scanning electron microscopy (SEM) technique was performed to observe surface morphology. As shown in Figure 3c,d, both films have identical surface morphology, which are densely packed by discrete QDs. Figure 3e shows the absorption and PL characteristics, in which there is no significant difference between C−$CsPbI_3$ and R−$CsPbI_3$ QD films. Additionally, carrier lifetime calculated from the time-resolved PL spectra using single-exponent fitting is also very similar, i.e., 4.5 ns for the C−$CsPbI_3$ and 4.2 ns for the R−$CsPbI_3$ QD films, which are on a par with reported results.[31,54] Therefore, both kinds of QD films demonstrate very similar characteristics, confirming the high feasibility of the proposed recycling process for producing reliable alternative lead sources.

First-principles density functional theory (DFT) calculations (Experimental section in the Supporting Information) revealed that the formation energy of Na interstitials, E_f, reaches the minimum when Na^+ resides on the top of the $CsPbI_3$ slab surface. Specifically, E_f is 3.11 eV for the Na^+ residing at the surface (Figure 4a), 3.43 eV for the Na^+ in the core of $CsPbI_3$

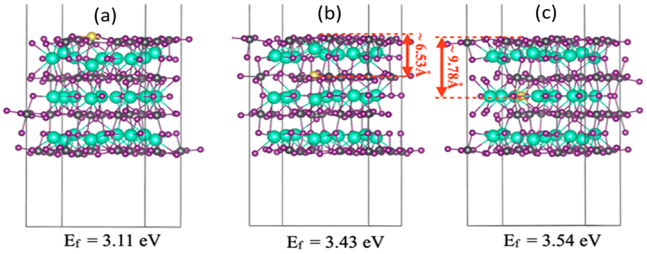

Figure 4. Optimized geometries and formation energies (E_f) of a Na^+ interstitial defect in a $CsPbI_3$ slab expressed as a function of distance to the surface. Black lines indicate the boundaries of the simulation cell employed in the first-principles DFT calculations. Cs, Pb, I, and Na atoms are represented with cyan, gray, purple, and yellow spheres, respectively.

QD with a distance of 6.53 Å from the surface (Figure 4b), and 3.54 eV for the Na^+ with a distance of 9.78 Å from the surface (Figure 4c). The location-dependent trend of E_f indicates that the interstitial Na atoms would migrate from the interior of the slab and prefer to stay at the $CsPbI_3$ QD surface. It is a general phenomenon that defects can be favorably excluded from the lattice of QDs because they are thermodynamically unstable in the host as a result of their high formation energy.[55] This calculation result also provides a clue for the energetics involved in doping impurity elements into perovskite nanocrystals. Clearly, the recycled lead source is more suitable for fabricating perovskite QDs than their bulk film counterparts as the self-purification effect can suppress the detrimental effects of impurities.

https://doi.org/10.1021/acsmaterialslett.1c00592
ACS Materials Lett. 2022, 4, 120−127

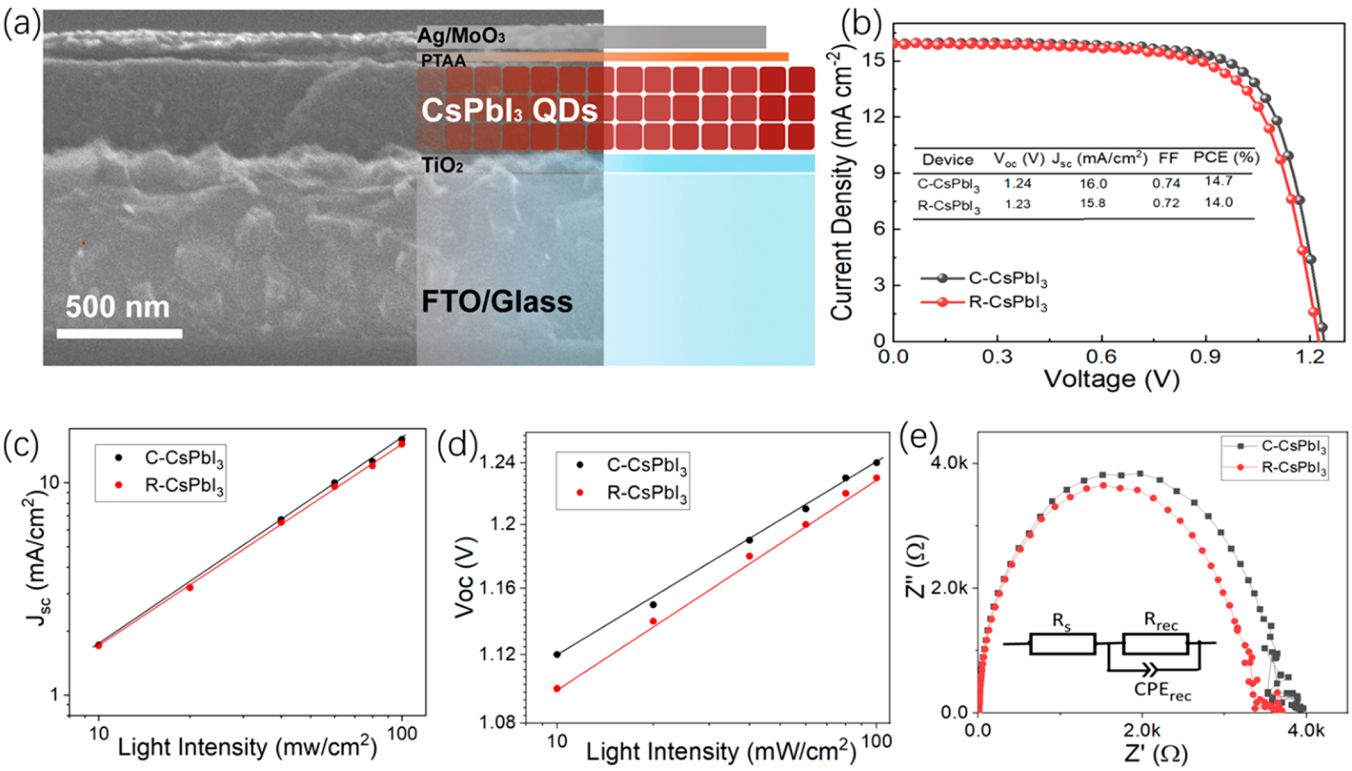

Figure 5. (a) Cross-sectional SEM image of the R−$CsPbI_3$ QD solar cell. (b) J−V curves. Light intensity dependence of (c) J_{SC} and (d) V_{OC} of both QD solar cells. (e) Corresponding EIS Nyquist plots of the champion devices of C−$CsPbI_3$ and R−$CsPbI_3$ QD solar cells.

Table 3. Summary of Performance Statistics for the $CsPbI_3$ Solar Cells[a]

device type	V_{OC} (V)	J_{SC} (mA cm^{-2})	FF	PCE (%)
C−$CsPbI_3$	1.22 ± 0.03 (1.24)	15.7 ± 0.6 (16.0)	0.72 ± 0.02 (0.74)	13.8 ± 0.5 (14.7)
R−$CsPbI_3$	1.22 ± 0.03 (1.23)	15.3 ± 0.7 (15.8)	0.71 ± 0.03 (0.72)	13.3 ± 0.5 (14.0)

[a]The champion parameters are in parentheses, and there are 24 devices for each type.

$CsPbI_3$ QD solar cells were fabricated using the structure of FTO/C−TiO_2/$CsPbI_3$/PTAA/MoO_3/Ag, where the sprayed TiO_2 compact layer serves as the electron transport layer, $CsPbI_3$ QDs as the light absorbing layer, and PTAA as the hole transport layer. The experimental details are given in the Supporting Information. Figure 5a shows the cross-sectional SEM image of a complete R−$CsPbI_3$ QD solar cell, and each layer can be clearly identified. Figure 5b demonstrates the current density−voltage (J−V) curves of the champion solar cells under the reverse scanning direction. The C−$CsPbI_3$ solar cell achieved a PCE of 14.7% with an open-circuit voltage (V_{oc}) of 1.24 V, a short-circuit current density (J_{sc}) of 16.0 mA/cm^2, and a fill factor (FF) of 0.74, while the R−$CsPbI_3$ solar cell delivered a comparable PCE of 14.0% with a V_{oc} of 1.23 V, a J_{sc} of 15.8 mA/cm^2, and an FF of 0.72. The performance statistics for two batches of solar cells are given in Table 3, and the average efficiency is 13.8% for the C−$CsPbI_3$ solar cells and 13.3% for the R−$CsPbI_3$ solar cells, which are comparable with the reported state-of-the-art values,[54] and a detailed comparison is given in Table S1. Additionally, as shown in Figure S2, the R−$CsPbI_3$ QD and C−$CsPbI_3$ cells delivered negligible hysteresis, which is in line with the reported results.[56]

To investigate the charge carrier generation and recombination mechanisms, we probed the recombination processes in both $CsPbI_3$ QD devices using the light intensity dependence of J_{sc} and V_{oc} measurements. The power-law dependence of J_{SC} with the light intensity generally obeys the relationship of $J_{SC} \propto I^{\alpha}$, where I is the light intensity and α is the exponential factor. As shown in Figure 5c, both cells exhibit α values close to unity, i.e., 0.98 for the C−$CsPbI_3$ device and 0.97 for the R−$CsPbI_3$ device, indicating that bimolecular recombination does not dominate in both $CsPbI_3$ QD devices. V_{oc} of the device at different light intensities was also recorded and given in Figure 5d. The slope of V_{oc} versus the light intensity follows nkT/q, where n, k, T, and q are the diode ideality factor, the Boltzmann constant, temperature, and the elementary charge, respectively. The larger diode ideality factor (n) is indicative of more trap-assisted recombination occurring in a cell at open-circuit condition. The slope of the C−$CsPbI_3$ device (1.19 kT/q) is also close to that of the R−$CsPbI_3$ device (1.21 kT/q), suggesting that the trap-assisted recombination in both devices is similar. Additionally, electrochemical impedance spectroscopy (EIS) was applied to study the $CsPbI_3$ QD devices. The Nyquist plots of C−$CsPbI_3$ and R−$CsPbI_3$ QD solar cells measured at 0 V under dark conditions are shown in Figure 5e, and the inset shows the equivalent circuit. The intersection between the spectra and the Z'-axis at high and low frequencies represent the series resistance (R_s) and the recombination resistance (R_{rec}) of the device, respectively. Since the charge transport layers are identical in both devices, the R_s and R_{rec} values are associated with the $CsPbI_3$ QD films.

https://doi.org/10.1021/acsmaterialslett.1c00592
ACS Materials Lett. 2022, 4, 120−127

The C−$CsPbI_3$ cell shows a R_s of 23.1 Ω and R_{rec} of 3745.3 Ω, as compared to R_s of 28.6 Ω and R_{rec} of 3635.8 Ω in the R−$CsPbI_3$ cell. The similar values of R_s and R_{rec} indicate that the quality of both QD films is very close, which is consistent with the similar photovoltaic performance in both cells.

In conclusion, the PbI_2 powder was successfully synthesized from the spent lead acid batteries by using a facile and efficient low-temperature one-pot method, which not only recycles the lead waste of spent batteries but also provides a low-cost and environment-friendly way to synthesize lead precursors. More importantly, we found that the recycled PbI_2 is suitable to synthesize perovskite QDs due to the self-purification effect, which leads to the expulsion of impurity atoms from the lattice of $CsPbI_3$ QDs. As a result, $CsPbI_3$ QDs synthesized from both recycled and commercial PbI_2 showed similar physical properties, including size distribution, PLQY, absorbance, and carrier lifetime. The resulting $CsPbI_3$ QD solar cells achieved PCE of 14.7% and 14.0% for the C−$CsPbI_3$ and R−$CsPbI_3$ QD devices, respectively. These results validate that the PbI_2 precursor recycled from spent lead acid batteries with the low-temperature solution process is suitable for QD-based optoelectronic applications.

■ ASSOCIATED CONTENT

Supporting Information

The Supporting Information is available free of charge at https://pubs.acs.org/doi/10.1021/acsmaterialslett.1c00592.

Experimental section including PbI_2 preparation, $CsPbI_3$ QD synthesis, and DFT simulations; SEM, XPS, and *J*−*V* curves; and table reporting state of the art efficiencies and device structures of $CsPbI_3$ QD solar cells (PDF)

■ AUTHOR INFORMATION

Corresponding Authors

Jianyu Yuan − *Institute of Functional Nano & Soft Materials (FUNSOM), Jiangsu Key Laboratory for Carbon-Based Functional Materials and Devices, Joint International Research Laboratory of Carbon-Based Functional Materials and Devices, Soochow University, Suzhou, Jiangsu 215123, China;* orcid.org/0000-0002-5131-1285; Email: jyyuan.suda.edu.cn

Tom Wu − *School of Materials Science and Engineering, University of New South Wales (UNSW), Sydney, New South Wales 2052, Australia;* orcid.org/0000-0003-0845-4827; Email: tom.wu@unsw.edu.au

Fangyang Liu − *School of Metallurgy and Environment, Central South University, Changsha 410083, China;* orcid.org/0000-0002-0580-7888; Email: liufangyang@csu.edu.cn

Authors

Long Hu − *School of Engineering, Macquarie University Sustainable Energy Research Centre, Macquarie University, Sydney, New South Wales 2109, Australia; School of Materials Science and Engineering, University of New South Wales (UNSW), Sydney, New South Wales 2052, Australia*

Qingya Li − *School of Metallurgy and Environment, Central South University, Changsha 410083, China*

Yuchen Yao − *School of Materials Science and Engineering, University of New South Wales (UNSW), Sydney, New South Wales 2052, Australia*

Qiang Zeng − *School of Metallurgy and Environment, Central South University, Changsha 410083, China; Yitai Technology Ltd., Changsha 410083, China*

Zizhen Zhou − *School of Materials Science and Engineering, University of New South Wales (UNSW), Sydney, New South Wales 2052, Australia*

Claudio Cazorla − *Departament de Física, Universitat Politècnica de Catalunya, E-08034 Barcelona, Spain;* orcid.org/0000-0002-6501-4513

Tao Wan − *School of Materials Science and Engineering, University of New South Wales (UNSW), Sydney, New South Wales 2052, Australia;* orcid.org/0000-0001-9345-8624

Xinwei Guan − *School of Materials Science and Engineering, University of New South Wales (UNSW), Sydney, New South Wales 2052, Australia;* orcid.org/0000-0002-0100-480X

Jing-Kai Huang − *School of Materials Science and Engineering, University of New South Wales (UNSW), Sydney, New South Wales 2052, Australia*

Chun-Ho Lin − *School of Materials Science and Engineering, University of New South Wales (UNSW), Sydney, New South Wales 2052, Australia;* orcid.org/0000-0003-0882-4728

Mengyao Li − *School of Materials Science and Engineering, University of New South Wales (UNSW), Sydney, New South Wales 2052, Australia*

Soshan Cheong − *Electron Microscope Unit, Mark Wainwright Analytical Centre, University of New South Wales (UNSW), Sydney, New South Wales 2052, Australia;* orcid.org/0000-0001-6133-0829

Richard D. Tilley − *Electron Microscope Unit, Mark Wainwright Analytical Centre, University of New South Wales (UNSW), Sydney, New South Wales 2052, Australia;* orcid.org/0000-0003-2097-063X

Dewei Chu − *School of Materials Science and Engineering, University of New South Wales (UNSW), Sydney, New South Wales 2052, Australia;* orcid.org/0000-0003-4581-0560

Shujuan Huang − *School of Engineering, Macquarie University Sustainable Energy Research Centre, Macquarie University, Sydney, New South Wales 2109, Australia;* orcid.org/0000-0003-3468-4773

Complete contact information is available at: https://pubs.acs.org/10.1021/acsmaterialslett.1c00592

Notes

The authors declare no competing financial interest.

■ ACKNOWLEDGMENTS

L. Hu, Y. Li, and Y. Yao equally contributed to this work. We acknowledge the support of the Australian Research Council (Grant DP190103316). This project is partially supported by the Australian Renewable Energy Agency (ARENA) via Projects 2020/RND001 and 2020/RND 003. J. Yuan thanks the support from the National Key Research and Development Program of China (Grant No. 2019YFE0108600), National Natural Science Foundation of China (Grant No. 52073198), Natural Science Foundation of Jiangsu Province (Grant BK20211598) "111" project, and Collaborative Innovation Center of Suzhou Nano Science and Technology, Soochow University. This work used the facilities supported by

Microscopy Australia at the Electron Microscope Unit at University of New South Wales.

■ REFERENCES

(1) Tang, J.; Kemp, K. W.; Hoogland, S.; Jeong, K. S.; Liu, H.; Levina, L.; Furukawa, M.; Wang, X.; Debnath, R.; Cha, D.; Chou, K. W.; Fischer, A.; Amassian, A.; Asbury, J. B.; Sargent, E. H. Colloidal-Quantum-Dot Photovoltaics Using Atomic-Ligand Passivation. *Nat. Mater.* **2011**, *10*, 765−771.

(2) Chuang, C. H.; Brown, P. R.; Bulovic, V.; Bawendi, M. G. Improved Performance and Stability in Quantum Dot Solar Cells through Band Alignment Engineering. *Nat. Mater.* **2014**, *13*, 796−801.

(3) Cao, Y.; Stavrinadis, A.; Lasanta, T.; So, D.; Konstantatos, G. The Role of Surface Passivation for Efficient and Photostable PbS Quantum Dot Solar Cells. *Nat. Energy* **2016**, *1*, 16035.

(4) Hu, L.; Geng, X.; Singh, S.; Shi, J.; Hu, Y.; Li, S.; Guan, X.; He, T.; Li, X.; Cheng, Z.; Patterson, R.; Huang, S.; Wu, T. Synergistic Effect of Electron Transport Layer and Colloidal Quantum Dot Solid Enable PbSe Quantum Dot Solar Cell Achieving over 10% Efficiency. *Nano Energy* **2019**, *64*, 103922.

(5) Kim, J.; Hu, L.; Chen, H.; Guan, X.; Anandan, P. R.; Li, F.; Tang, J.; Lin, C.-H.; Kalantar-Zadeh, K.; Tricoli, A.; Wu, T. P-Type Charge Transport and Selective Gas Sensing of All-Inorganic Perovskite Nanocrystals. *ACS Mater. Lett.* **2020**, *2*, 1368−1374.

(6) Liu, S.; Hu, L.; Huang, S.; Zhang, W.; Ma, J.; Wang, J.; Guan, X.; Lin, C. H.; Kim, J.; Wan, T.; Lei, Q.; Chu, D.; Wu, T. Enhancing the Efficiency and Stability of PbS Quantum Dot Solar Cells through Engineering an Ultrathin NiO Nanocrystalline Interlayer. *ACS Appl. Mater. Interfaces* **2020**, *12*, 46239−46246.

(7) Hu, L.; Lei, Q.; Guan, X.; Patterson, R.; Yuan, J.; Lin, C. H.; Kim, J.; Geng, X.; Younis, A.; Wu, X.; Liu, X.; Wan, T.; Chu, D.; Wu, T.; Huang, S. Optimizing Surface Chemistry of PbS Colloidal Quantum Dot for Highly Efficient and Stable Solar Cells Via Chemical Binding. *Adv. Sci.* **2021**, *8*, 2003138.

(8) Duan, L.; Hu, L.; Guan, X.; Lin, C. H.; Chu, D.; Huang, S.; Liu, X.; Yuan, J.; Wu, T. Quantum Dots for Photovoltaics: A Tale of Two Materials. *Adv. Energy Mater.* **2021**, *11*, 2100354.

(9) Hu, L.; Guan, X.; Chen, W.; Yao, Y.; Wan, T.; Lin, C.-H.; Pham, N. D.; Yuan, L.; Geng, X.; Wang, F.; Huang, C.-Y.; Yuan, J.; Cheong, S.; Tilley, R. D.; Wen, X.; Chu, D.; Huang, S.; Wu, T. Linking Phase Segregation and Photovoltaic Performance of Mixed-Halide Perovskite Films through Grain Size Engineering. *ACS Energy Lett.* **2021**, *6*, 1649−1658.

(10) Eita, M.; Usman, A.; El-Ballouli, A. O.; Alarousu, E.; Bakr, O. M.; Mohammed, O. F. A Layer-by-Layer ZnO Nanoparticle-PbS Quantum Dot Self-Assembly Platform for Ultrafast Interfacial Electron Injection. *Small* **2015**, *11*, 112−118.

(11) Carey, G. H.; Abdelhady, A. L.; Ning, Z.; Thon, S. M.; Bakr, O. M.; Sargent, E. H. Colloidal Quantum Dot Solar Cells. *Chem. Rev.* **2015**, *115*, 12732−12763.

(12) El-Ballouli, A. O.; Alarousu, E.; Usman, A.; Pan, J.; Bakr, O. M.; Mohammed, O. F. Real-Time Observation of Ultrafast Intraband Relaxation and Exciton Multiplication in PbS Quantum Dots. *ACS Photonics* **2014**, *1*, 285−292.

(13) Bertens, K.; Fan, J. Z.; Biondi, M.; Rasouli, A. S.; Lee, S.; Li, P.; Sun, B.; Hoogland, S.; García de Arquer, F. P.; Lu, Z.-H.; Sargent, E. H. Colloidal Quantum Dot Solar Cell Band Alignment Using Two-Step Ionic Doping. *ACS Mater. Lett.* **2020**, *2*, 1583−1589.

(14) Gaulding, E. A.; Chen, X.; Yang, Y.; Harvey, S. P.; To, B.; Kim, Y.-H.; Beard, M. C.; Sercel, P. C.; Luther, J. M. Embedding PbS Quantum Dots (QDs) in Pb-Halide Perovskite Matrices: QD Surface Chemistry and Antisolvent Effects on QD Dispersion and Confinement Properties. *ACS Mater. Lett.* **2020**, *2*, 1464−1472.

(15) Pradhan, S.; Stavrinadis, A.; Gupta, S.; Christodoulou, S.; Konstantatos, G. Breaking the Open-Circuit Voltage Deficit Floor in PbS Quantum Dot Solar Cells through Synergistic Ligand and Architecture Engineering. *ACS Energy Lett.* **2017**, *2*, 1444−1449.

(16) Albaladejo-Siguan, M.; Becker-Koch, D.; Taylor, A. D.; Sun, Q.; Lami, V.; Oppenheimer, P. G.; Paulus, F.; Vaynzof, Y. Efficient and Stable PbS Quantum Dot Solar Cells by Triple-Cation Perovskite Passivation. *ACS Nano* **2020**, *14*, 384−393.

(17) Sun, B.; Johnston, A.; Xu, C.; Wei, M.; Huang, Z.; Jiang, Z.; Zhou, H.; Gao, Y.; Dong, Y.; Ouellette, O.; Zheng, X.; Liu, J.; Choi, M.-J.; Gao, Y.; Baek, S.-W.; Laquai, F.; Bakr, O. M.; Ban, D.; Voznyy, O.; García de Arquer, F. P.; Sargent, E. H. Monolayer Perovskite Bridges Enable Strong Quantum Dot Coupling for Efficient Solar Cells. *Joule* **2020**, *4*, 1542−1556.

(18) Ahmad, W.; He, J.; Liu, Z.; Xu, K.; Chen, Z.; Yang, X.; Li, D.; Xia, Y.; Zhang, J.; Chen, C. Lead Selenide (PbSe) Colloidal Quantum Dot Solar Cells with > 10% Efficiency. *Adv. Mater.* **2019**, *31*, 1900593.

(19) Liu, Y.; Li, F.; Shi, G.; Liu, Z.; Lin, X.; Shi, Y.; Chen, Y.; Meng, X.; Lv, Y.; Deng, W.; Pan, X.; Ma, W. PbSe Quantum Dot Solar Cells Based on Directly Synthesized Semiconductive Inks. *ACS Energy Lett.* **2020**, *5*, 3797−3803.

(20) Swarnkar, A.; Marshall, A. R.; Sanehira, E. M.; Chernomordik, B. D.; Moore, D. T.; Christians, J. A.; Chakrabarti, T.; Luther, J. M. Quantum Dot-Induced Phase Stabilization of Alpha-$CsPbI_3$ Perovskite for High-Efficiency Photovoltaics. *Science* **2016**, *354*, 92−95.

(21) Liu, F.; Zhang, Y.; Ding, C.; Kobayashi, S.; Izuishi, T.; Nakazawa, N.; Toyoda, T.; Ohta, T.; Hayase, S.; Minemoto, T.; Yoshino, K.; Dai, S.; Shen, Q. Highly Luminescent Phase-Stable $CsPbI_3$ Perovskite Quantum Dots Achieving near 100% Absolute Photoluminescence Quantum Yield. *ACS Nano* **2017**, *11*, 10373−10383.

(22) Zhou, W.; Shang, Y.; García de Arquer, F. P.; Xu, K.; Wang, R.; Luo, S.; Xiao, X.; Zhou, X.; Huang, R.; Sargent, E. H.; Ning, Z. Solution-Processed Upconversion Photodetectors Based on Quantum Dots. *Nat. Electron.* **2020**, *3*, 251−258.

(23) Mao, W.; Hall, C. R.; Bernardi, S.; Cheng, Y. B.; Widmer-Cooper, A.; Smith, T. A.; Bach, U. Light-Induced Reversal of Ion Segregation in Mixed-Halide Perovskites. *Nat. Mater.* **2021**, *20*, 55−61.

(24) Zheng, X.; Yuan, S.; Liu, J.; Yin, J.; Yuan, F.; Shen, W.-S.; Yao, K.; Wei, M.; Zhou, C.; Song, K.; Zhang, B.-B.; Lin, Y.; Hedhili, M. N.; Wehbe, N.; Han, Y.; Sun, H.-T.; Lu, Z.-H.; Anthopoulos, T. D.; Mohammed, O. F.; Sargent, E. H.; Liao, L.-S.; Bakr, O. M. Chlorine Vacancy Passivation in Mixed Halide Perovskite Quantum Dots by Organic Pseudohalides Enables Efficient Rec. 2020 Blue Light-Emitting Diodes. *ACS Energy Lett.* **2020**, *5*, 793−798.

(25) Younis, A.; Lin, C. H.; Guan, X.; Shahrokhi, S.; Huang, C. Y.; Wang, Y.; He, T.; Singh, S.; Hu, L.; Retamal, J. R. D.; He, J. H.; Wu, T. Halide Perovskites: A New Era of Solution-Processed Electronics. *Adv. Mater.* **2021**, *33*, 2005000.

(26) Hao, M.; Bai, Y.; Zeiske, S.; Ren, L.; Liu, J.; Yuan, Y.; Zarrabi, N.; Cheng, N.; Ghasemi, M.; Chen, P.; Lyu, M.; He, D.; Yun, J.-H.; Du, Y.; Wang, Y.; Ding, S.; Armin, A.; Meredith, P.; Liu, G.; Cheng, H.-M.; Wang, L. Ligand-Assisted Cation-Exchange Engineering for High-Efficiency Colloidal $Cs_{1-x}FA_xPbI_3$ Quantum Dot Solar Cells with Reduced Phase Segregation. *Nat. Energy* **2020**, *5*, 79−88.

(27) Ma, J.-P.; Chen, J.-K.; Yin, J.; Zhang, B.-B.; Zhao, Q.; Kuroiwa, Y.; Moriyoshi, C.; Hu, L.; Bakr, O. M.; Mohammed, O. F.; Sun, H.-T. Doping Induces Structural Phase Transitions in All-Inorganic Lead Halide Perovskite Nanocrystals. *ACS Mater. Lett.* **2020**, *2*, 367−375.

(28) Hu, L.; Zhao, Q.; Huang, S.; Zheng, J.; Guan, X.; Patterson, R.; Kim, J.; Shi, L.; Lin, C. H.; Lei, Q.; Chu, D.; Tao, W.; Cheong, S.; Tilley, R. D.; Ho-Baillie, A. W. Y.; Luther, J. M.; Yuan, J.; Wu, T. Flexible and Efficient Perovskite Quantum Dot Solar Cells Via Hybrid Interfacial Architecture. *Nat. Commun.* **2021**, *12*, 466.

(29) Khan, J.; Zhang, X.; Yuan, J.; Wang, Y.; Shi, G.; Patterson, R.; Shi, J.; Ling, X.; Hu, L.; Wu, T.; Dai, S.; Ma, W. Tuning the Surface-Passivating Ligand Anchoring Position Enables Phase Robustness in $CsPbI_3$ Perovskite Quantum Dot Solar Cells. *ACS Energy Lett.* **2020**, *5*, 3322−3329.

(30) Zhang, L.; Kang, C.; Zhang, G.; Pan, Z.; Huang, Z.; Xu, S.; Rao, H.; Liu, H.; Wu, S.; Wu, X.; Li, X.; Zhu, Z.; Zhong, X.; Jen, A. K.-Y.

All-Inorganic $CsPbI_3$ Quantum Dot Solar Cells with Efficiency over 16% by Defect Control. *Adv. Funct. Mater.* **2021**, *31*, 2005930.

(31) Jia, D.; Chen, J.; Yu, M.; Liu, J.; Johansson, E. M. J.; Hagfeldt, A.; Zhang, X. Dual Passivation of $CsPbI_3$ Perovskite Nanocrystals with Amino Acid Ligands for Efficient Quantum Dot Solar Cells. *Small* **2020**, *16*, 2001772.

(32) Hsu, B. W.; Chuang, Y. T.; Cheng, C. Y.; Chen, C. Y.; Chen, Y. J.; Brumberg, A.; Yang, L.; Huang, Y. S.; Schaller, R. D.; Chen, L. J.; Chuu, C. S.; Lin, H. W. Very Robust Spray-Synthesized $CsPbI_3$ Quantum Emitters with Ultrahigh Room-Temperature Cavity-Free Brightness and Self-Healing Ability. *ACS Nano* **2021**, *15*, 11358−11368.

(33) Ling, X.; Yuan, J.; Zhang, X.; Qian, Y.; Zakeeruddin, S. M.; Larson, B. W.; Zhao, Q.; Shi, J.; Yang, J.; Ji, K.; Zhang, Y.; Wang, Y.; Zhang, C.; Duhm, S.; Luther, J. M.; Gratzel, M.; Ma, W. Guanidinium-Assisted Surface Matrix Engineering for Highly Efficient Perovskite Quantum Dot Photovoltaics. *Adv. Mater.* **2020**, *32*, 2001906.

(34) Jia, D.; Chen, J.; Mei, X.; Fan, W.; Luo, S.; Yu, M.; Liu, J.; Zhang, X. Surface Matrix Curing of Inorganic $CsPbI_3$ Perovskite Quantum Dots for Solar Cells with Efficiency over 16. *Energy Environ. Sci.* **2021**, *14*, 4599−4609.

(35) Wang, Y.; Jia, B.; Wang, J.; Xue, P.; Xiao, Y.; Li, T.; Wang, J.; Lu, H.; Tang, Z.; Lu, X.; Huang, F.; Zhan, X. High-Efficiency Perovskite Quantum Dot Hybrid Nonfullerene Organic Solar Cells with near-Zero Driving Force. *Adv. Mater.* **2020**, *32*, No. 2002066.

(36) Zhao, Q.; Hazarika, A.; Chen, X.; Harvey, S. P.; Larson, B. W.; Teeter, G. R.; Liu, J.; Song, T.; Xiao, C.; Shaw, L.; Zhang, M.; Li, G.; Beard, M. C.; Luther, J. M. High Efficiency Perovskite Quantum Dot Solar Cells with Charge Separating Heterostructure. *Nat. Commun.* **2019**, *10*, 2842.

(37) Zhang, X.; Li, L.; Fan, E.; Xue, Q.; Bian, Y.; Wu, F.; Chen, R. Toward Sustainable and Systematic Recycling of Spent Rechargeable Batteries. *Chem. Soc. Rev.* **2018**, *47*, 7239−7302.

(38) Chen, P.-Y.; Qi, J.; Klug, M. T.; Dang, X.; Hammond, P. T.; Belcher, A. M. Environmentally Responsible Fabrication of Efficient Perovskite Solar Cells from Recycled Car Batteries. *Energy Environ. Sci.* **2014**, *7*, 3659−3665.

(39) Li, M.; Yang, J.; Liang, S.; Hou, H.; Hu, J.; Liu, B.; Kumar, R. V. Review on Clean Recovery of Discarded/Spent Lead-Acid Battery and Trends of Recycled Products. *J. Power Sources* **2019**, *436*, 226853.

(40) Li, C.; Zhu, Z.; Wang, Y.; Guo, Q.; Wang, C.; Zhong, P.; Tan, Z. a.; Yang, R. Lead Acetate Produced from Lead-Acid Battery for Efficient Perovskite Solar Cells. *Nano Energy* **2020**, *69*, 104380.

(41) Dalpian, G. M.; Chelikowsky, J. R. Self-Purification in Semiconductor Nanocrystals. *Phys. Rev. Lett.* **2006**, *96*, 226802.

(42) Pan, J.; Sun, Y.; Li, W.; Knight, J.; Manthiram, A. A Green Lead Hydrometallurgical Process Based on a Hydrogen-Lead Oxide Fuel Cell. *Nat. Commun.* **2013**, *4*, 2178.

(43) Xu, J.; Hu, Z.; Huang, L.; Huang, X.; Jia, X.; Zhang, J.; Zhang, J.; Zhu, Y. In Situ Recycle of PbI_2 as a Step Towards Sustainable Perovskite Solar Cells. *Prog. Photovoltaics* **2017**, *25*, 1022−1033.

(44) Chhillar, P.; Dhamaniya, B. P.; Dutta, V.; Pathak, S. K. Recycling of Perovskite Films: Route toward Cost-Efficient and Environment-Friendly Perovskite Technology. *ACS Omega* **2019**, *4*, 11880−11887.

(45) Kim, B. J.; Kim, D. H.; Kwon, S. L.; Park, S. Y.; Li, Z.; Zhu, K.; Jung, H. S. Selective Dissolution of Halide Perovskites as a Step Towards Recycling Solar Cells. *Nat. Commun.* **2016**, *7*, 11735.

(46) Feng, X.; Guo, Q.; Xiu, J.; Ying, Z.; Ng, K. W.; Huang, L.; Wang, S.; Pan, H.; Tang, Z.; He, Z. Close-Loop Recycling of Perovskite Solar Cells through Dissolution-Recrystallization of Perovskite by Butylamine. *Cell Rep. Phys. Sci.* **2021**, *2*, 100341.

(47) Ghosh, D.; Chaudhary, D. K.; Ali, M. Y.; Chauhan, K. K.; Prodhan, S.; Bhattacharya, S.; Ghosh, B.; Datta, P. K.; Ray, S. C.; Bhattacharyya, S. All-Inorganic Quantum Dot Assisted Enhanced Charge Extraction across the Interfaces of Bulk Organo-Halide Perovskites for Efficient and Stable Pin-Hole Free Perovskite Solar Cells. *Chem. Sci.* **2019**, *10*, 9530−9541.

(48) Senevirathna, D. C.; Yu, J. C.; Nirmal Peiris, T. A.; Li, B.; Michalska, M.; Li, H.; Jasieniak, J. J. Impact of Anion Impurities in Commercial PbI_2 on Lead Halide Perovskite Films and Solar Cells. *ACS Mater. Lett.* **2021**, *3*, 351−355.

(49) Yavari, M.; Ebadi, F.; Meloni, S.; Wang, Z. S.; Yang, T. C.-J.; Sun, S.; Schwartz, H.; Wang, Z.; Niesen, B.; Durantini, J.; Rieder, P.; Tvingstedt, K.; Buonassisi, T.; Choy, W. C. H.; Filippetti, A.; Dittrich, T.; Olthof, S.; Correa-Baena, J.-P.; Tress, W. How Far Does the Defect Tolerance of Lead-Halide Perovskites Range? The Example of Bi Impurities Introducing Efficient Recombination Centers. *J. Mater. Chem. A* **2019**, *7*, 23838−23853.

(50) Bai, B.; Xu, M.; Li, J.; Zhang, S.; Qiao, C.; Liu, J.; Zhang, J. Dopant Diffusion Equilibrium Overcoming Impurity Loss of Doped QDs for Multimode Anti-Counterfeiting and Encryption. *Adv. Funct. Mater.* **2021**, *31*, 2100286.

(51) Zolfaghari, Z.; Hassanabadi, E.; Pitarch-Tena, D.; Yoon, S. J.; Shariatinia, Z.; van de Lagemaat, J.; Luther, J. M.; Mora-Seró, I. Operation Mechanism of Perovskite Quantum Dot Solar Cells Probed by Impedance Spectroscopy. *ACS Energy Lett.* **2019**, *4*, 251−258.

(52) Tong, Y.; Bladt, E.; Ayguler, M. F.; Manzi, A.; Milowska, K. Z.; Hintermayr, V. A.; Docampo, P.; Bals, S.; Urban, A. S.; Polavarapu, L.; Feldmann, J. Highly Luminescent Cesium Lead Halide Perovskite Nanocrystals with Tunable Composition and Thickness by Ultrasonication. *Angew. Chem., Int. Ed.* **2016**, *55*, 13887−13892.

(53) Chen, K.; Jin, W.; Zhang, Y.; Yang, T.; Reiss, P.; Zhong, Q.; Bach, U.; Li, Q.; Wang, Y.; Zhang, H.; Bao, Q.; Liu, Y. High Efficiency Mesoscopic Solar Cells Using $CsPbI_3$ Perovskite Quantum Dots Enabled by Chemical Interface Engineering. *J. Am. Chem. Soc.* **2020**, *142*, 3775−3783.

(54) Yuan, J.; Zhang, X.; Sun, J.; Patterson, R.; Yao, H.; Xue, D.; Wang, Y.; Ji, K.; Hu, L.; Huang, S.; Chu, D.; Wu, T.; Hou, J.; Yuan, J. Hybrid Perovskite Quantum Dot/Non-Fullerene Molecule Solar Cells with Efficiency over 15%. *Adv. Funct. Mater.* **2021**, *31*, 2101272.

(55) Stavrinadis, A.; Konstantatos, G. Strategies for the Controlled Electronic Doping of Colloidal Quantum Dot Solids. *ChemPhysChem* **2016**, *17*, 632−644.

(56) Wang, Y.; Yuan, J.; Zhang, X.; Ling, X.; Larson, B. W.; Zhao, Q.; Yang, Y.; Shi, Y.; Luther, J. M.; Ma, W. Surface Ligand Management Aided by a Secondary Amine Enables Increased Synthesis Yield of $CsPbI_3$ Perovskite Quantum Dots and High Photovoltaic Performance. *Adv. Mater.* **2020**, *32*, 2000449.

https://doi.org/10.1021/acsmaterialslett.1c00592
ACS Materials Lett. 2022, 4, 120−127